HHS Public Access

Author manuscript

Genesis. Author manuscript; available in PMC 2020 January 01.

Published in final edited form as:

Genesis. 2019 January ; 57(1): e23252. doi:10.1002/dvg.23252.

A requirement for *Fgfr2* in middle ear development

Diana Rigueur[#1,2], **Ryan R. Roberts**[#1,2], **Lauren Bobzin**[1,2], and **Amy E. Merrill**[1,2,*]

[1]Center for Craniofacial Molecular Biology, Ostrow School of Dentistry, University of Southern California, Los Angeles, CA, 90033

[2]Department of Biochemistry and Molecular Medicine, Keck School of Medicine, University of Southern California, Los Angeles, CA, 90033

[#] These authors contributed equally to this work.

Abstract

The skeletal structure of the mammalian middle ear, which is composed of three endochondral ossicles suspended within a membranous air-filled capsule, plays a critical role in conducting sound. Gene mutations that alter skeletal development in the middle ear result in auditory impairment. Mutations in Fibroblast Growth Factor Receptor 2 (*FGFR2*), an important regulator of endochondral and intramembranous bone formation, cause a spectrum of congenital skeletal disorders featuring conductive hearing loss. While the middle ear malformations in multiple *FGFR2* gain-of-function disorders are clinically characterized, those in the *FGFR2* loss-of-function disorder Lacrimo-auriculo-dento-digital (LADD) syndrome are relatively undescribed. To better understand conductive hearing loss in LADD, we examined the middle ear skeleton of mice with conditional loss of *Fgfr2*. We find that decreased auditory function in *Fgfr2* mutant mice correlates with hypoplasia of the auditory bulla and ectopic bone growth at sites of tendon/ligament attachment. We show that ectopic bone associated with the intra-articular ligaments of the incudomalleal joint is derived from Scx-expressing cells and preceded by decreased expression of the joint progenitor marker *Gdf5*. Together, these results identify a role for *Fgfr2* in development of the middle ear skeletal tissues and suggest potential causes for conductive hearing loss in LADD syndrome.

Keywords

auditory ossicles; Fgfr2; joint development; skeletal development; craniofacial development

INTRODUCTION

A defining feature of mammals is the skeletal structure of the middle ear, which is composed of three endochondral ossicles (malleus, incus, and stapes) suspended within the air-filled membranous bone capsule of the auditory bulla. The chain-like configuration of the three ossicles is critical for mammalian auditory function. When sound funneled through the ear canal strikes the tympanic membrane, the malleus, incus, and stapes vibrate in succession to

[*]Correspondence: amerrill@usc.edu.

generate mechanical forces that induce a neurosensory response in the inner ear. The ability of the ossicles to transform sound into mechanical forces relies on the synovial joints between bones, the tendons connecting muscle to bone, and the ligaments suspending the bones within the auditory bulla.

Auditory function relies on proper development of the middle ear skeleton. Congenital disorders that alter the number, morphology, or configuration of the ossicles and/or the size and shape of the auditory bulla lead to conductive hearing loss (Bartel-Friedrich and Wulke, 2007). The causes of such alterations include mutations in genes that regulate development of bone, cartilage, and joint connective tissue (Mori-Akiyama *et al.*, 2003; Settle *et al.*, 2003; Trokovic *et al.*, 2003). Mutations in Fibroblast Growth Factor Receptor 2 (*FGFR2*), an important developmental regulator of skeletal development in the craniofacial complex, result in a spectrum of congenital syndromes that present with varying degrees of conductive hearing loss. *FGFR2* gain-of-function mutations in Apert, Crouzon, and Pfeiffer syndromes lead to hypoplasia and fixation of the ossicles, as well as morphologic abnormalities in the auditory bulla and external ear (Peterson-Falzone, 1981) (Zhou *et al.*, 2009) (Orvidas *et al.*, 1999) (Desai *et al.*, 2010; Vallino-Napoli, 1996). While there are numerous otologic characterizations of the *FGFR2* gain-of-function disorders, the abnormalities that cause conductive hearing loss in the *FGFR2* loss-of-function disorder Lacrimo-auriculo-dental-digital (LADD) syndrome remain relatively unknown (Hollister *et al.*, 1973; Rohmann *et al.*, 2006; Thompson *et al.*, 1985).

Skeletal tissues of the mammalian middle ear largely develop from neural crest cells (NCCs). NCCs that migrate into the first pharyngeal arch form the auditory bulla, malleus, and incus (Hall and Miyake, 2000; Rijli *et al.*, 1993; Richter *et al.*, 2010; Mallo and Gridley, 1996), while the NCCs that migrate into the second pharyngeal arch form the crura of the stapes (O'Gorman, 2005; Thompson *et al.*, 2012). The base of the stapes, on the other hand, develops from a cartilage condensation that is dually derived from NCCs and mesoderm (Thompson *et al.*, 2012; Minoux *et al.*, 2013; O'Gorman, 2005). While NCCs are believed to give rise to the dense connective tissues that make up the ossicular joint capsules, tendons, and ligaments, detailed lineage tracing of these tissues has not yet been reported. Using a genetic mouse model with conditional loss of *Fgfr2* in NCCs, we show that Fgfr2 regulates development of the middle ear skeleton. We find that conditional knockout (cKO) of *Fgfr2* in NCCs leads to multiple anomalies in the auditory bulla and ossicular chain, including ectopic bone within the incudomalleal joint at attachment sites for dense connective tissue. We demonstrate that these abnormalities in the middle ear skeleton correlate with reduced auditory function in *Fgfr2* mutant mice. Together our results suggest an explanation for conductive hearing loss in LADD syndrome.

RESULTS

NCC-specific inactivation of *Fgfr2* results in reduced auditory function

To determine the role of Fgfr2 in middle ear function, we conditionally inactivated *Fgfr2* in NCCs by crossing the $Fgfr2^{flx}$ conditional allele with the *Wnt1-Cre* driver (Yu *et al.*, 2003). To evaluate hearing in *Wnt1-Cre;* $Fgfr2^{flx/flx}$ mice, we measured Auditory Brainstem Response (ABR) thresholds at postnatal day 30 (P30). The ABR thresholds of inbred mice

typically range between 30–40 decibels (dB) (Zhou *et al.*, 2006). In our control mice, mean ABR thresholds measured within this range at sound frequencies of 8 kHz, 12 kHz, 16 kHz, 24 kHz, and 32 kHz (Figure 1) (n=5). At 4 kHz, the mean ABR threshold measured outside the average range at 50 dB, which can be explained by strain-related differences in hearing sensitivity (Willott and Turner, 1999). In *Wnt1-Cre; Fgfr2*$^{flx/flx}$ mice, ABR thresholds measured significantly higher at all frequencies measured compared to controls (Figure 1) (n=6). These results show that the *Wnt1-Cre; Fgfr2*$^{flx/flx}$ mice require an almost 2-fold increase in sound volume (dB) as compared to control mice in order to hear the same sound frequency. Furthermore, this result suggests that the structural defects observed in the middle ear of *Wnt1-Cre; Fgfr2*$^{flx/flx}$ mice are linked to hearing loss.

cKO of *Fgfr2* induces abnormalities in the auditory bulla

To examine the effects of Fgfr2 on development of the overall structure of the middle ear skeleton, we performed μCT analysis. At P30, the structure of the auditory bulla, the membranous capsule that encloses the air-filled cavity of the middle ear, was small and flat in *Wnt1-Cre; Fgfr2*$^{flx/flx}$ mice as compared to littermate controls (Figure 2 A–D) (n=3 littermate pairs). Morphometric measurements of the auditory canal showed that the area, normalized to the overall skull size, was significantly decreased in *Wnt1-Cre; Fgfr2*$^{flx/flx}$ mice compared to littermate controls (Figure 2 E). This indicates that shaped changes in the mutant auditory bulla were at least in part independent of the overall reduction in skull size. Measurements of the auditory bulla showed that the overall volume was significantly reduced in *Wnt1-Cre; Fgfr2*$^{flx/flx}$ mice compared to littermate controls (Figure 2 F).

The auditory bulla is a compound skeletal structure formed by fusion of multiple membranous bones, including the neural crest-derived tympanic ring and retrotympanic process (Richter *et al.*, 2010). To characterize the individual contributions of the tympanic ring and retrotympanic process to the auditory bulla, μCT surface renderings were utilized. At P30, the retrotympanic process (pseudo-colored blue) and tympanic ring (pseudo-colored red) were dysmorphic and hypoplastic in *Wnt1-Cre; Fgfr2*$^{flx/flx}$ mice (Figure 3 A, B). Differences in the retrotympanic process and tympanic ring were evident as early as P5, prior to the fusion of these bones into the auditory bulla (Figure 3 C, D) (n= 3 littermate pairs). These data suggest that the morphological defects in the auditory bulla of *Wnt1-Cre; Fgfr2*$^{flx/flx}$ mice are at least in part due to abnormal patterning of the retrotympanic process and tympanic ring.

cKO of *Fgfr2* leads to abnormalities in the middle ear air space.

Sound conduction through the middle ear depends on formation of an air-filled spaced within the auditory bulla. Failure to form the middle ear air space causes partial or complete hearing loss (Richter *et al.*, 2010). Since a reduction in the size of the auditory bulla is correlated with deficient middle ear air space (Cordas *et al.*, 2012; Richter *et al.*, 2010; Xu *et al.*, 1999), we examined the middle ear cavity of *Wnt1-Cre; Fgfr2*$^{flx/flx}$ mice. Orthogonal μCT sections at P30 identified an air-filled space (dark areas) in the external and middle ear of controls (Figure 4 A) (n=3 mice). In *Wnt1-Cre; Fgfr2*$^{flx/flx}$ mice, the overall air space was reduced in size and abnormally shaped, lacking a clear demarcation between the external and middle ear (Figure 4 B) (n=3 mice). Abnormalities in the ear air space can be explained

by truncations in the tympanic ring, which normally limits the medial extension of the external ear cavity (Aimi, 1983). It was also noted that the malleus of *Wnt1-Cre; Fgfr2*$^{flx/flx}$ mice abutted the bony capsule of the cochlea (Figure 4 A, B, arrowhead). Histological sections stained with Hematoxylin-Eosin at P13 confirmed the μCT findings in the mutant: the external and middle ear air spaces were reduced in size causing the manubrium of the malleus to be in direct contact with the cochlea (Figure 4 C, D, asterisks, arrowhead). Formation of the middle ear air space occurs by cavitation between P6–14, when neural crest-derived mesenchyme retracts from the tympanic membrane and ossicles (Richter *et al.*, 2010). At P13, *Wnt1-Cre; Fgfr2*$^{flx/flx}$ mice showed mesenchymal adhesion between the tympanic membrane and malleus (Figure 4 C, D, arrow). These results indicate that a reduction in the size of the middle ear space in *Wnt1-Cre; Fgfr2*$^{flx/flx}$ mice is correlated with spatial confinement of the malleus and incomplete cavitation.

cKO of *Fgfr2* results in ectopic bone formation on the middle ear ossicles

The ossicular chain plays a central role in transmitting sound vibrations from the tympanic membrane to the inner ear. Malformations in the ossicles that alter the continuity of the chain or its connections with the surrounding auditory bulla often result in hearing loss. To investigate the extent to which the ossicular malformations contribute to hearing loss in *Wnt1-Cre; Fgfr2*$^{flx/flx}$ mice, we examined their morphology. μCT at P30 identified ectopic bone formation at discrete regions along the ossicular chain of *Wnt1-Cre; Fgfr2*$^{flx/flx}$ mice. On the malleus, we observed ectopic bone on the manubrium where it attaches to the tympanic membrane (Figure 5 A, B, arrowhead) (n=3). Ectopic bone was also found at the ligament insertion site on the anterior process and on the stapes at the insertion site for the stapedius muscle (Figure 5 A, B, open arrowheads). Additionally, a discrete ectopic bone formation was seen within the incudomalleal joint (Figure 5 A, B>, arrow). Whole mount skeletal staining at P30 confirmed the presence of ectopic bone in these regions and identified ectopic bone on the malleus at the insertion site for the tensor tympani muscle and on the incus adjacent to the incudostapedial joint (Figure 5 C, D, open arrowheads) (n=3). Whole mount skeletal staining at P10 showed Alcian blue stain in many of the regions of ectopic bone (Figure 5 E, F) (n=3). Interestingly, the ectopic bone at the incudomalleal joint presented as a distinct endochondral-like element (Figure 5 F, arrow). Together these results demonstrate that loss of *Fgfr2* induces formation of ectopic endochondral-like bone in the middle ear at sites of joint articulation and tendon/ligament insertion. Ectopic bone in these regions is expected to impact ossicular chain continuity and/or suspension.

cKO of *Fgfr2* disrupts specification of the incudomalleal joint

To further characterize the ectopic bone at the incudomalleal joint of *Wnt1-Cre; Fgfr2*$^{flx/flx}$ mice, we analyzed histological sections treated with with Hall-Brunt Quadruple (HBQ) stain (Hall, 1986). The mature incudomalleal joint is V-shaped, with the articular surface of the incus forming a wedge that fits into a notch on the malleus (Amin and Tucker, 2006). In control mice at P9, the incudomalleal joint exhibited this typical V-shape and the articular cartilage of the incus and malleus were separated by a small group of fibroblast-like cells at the apex of the incus (Figure 6 A, A', arrow). In *Wnt1-Cre; Fgfr2*$^{flx/flx}$ mice, the joint shape was disrupted and the articular surfaces of the incus and malleus were separated by an ectopic piece of cartilage well-circumscribed by a superficial layer of flat fibroblast-like

cells (Figure 6 C, C', asterisk) (n=4). In addition, cavitation of mesenchyme surrounding the incus and malleus was relatively incomplete in *Wnt1-Cre; Fgfr2*$^{flx/flx}$ mice compared to controls (Figure 6 A, C). In control mice at P7, the articular surfaces of the incus and malleus were less defined and separated by cells of the joint interzone (Figure 6 B, B', arrow). In *Wnt1-Cre; Fgfr2*$^{flx/flx}$ mice, joint interzone cells were absent and the ectopic piece of cartilage was in close association with the articular surfaces of the incus and malleus (Figure 6 D, D', asterisk) (n=4). These findings indicate that *Fgfr2* regulates development of the incudomalleal joint.

The malleus and incus develop from a single chondrogenic condensation that is subdivided around E15.5 when cells within the presumptive joint region down-regulate cartilage markers in favor of joint specification genes such as *Gdf5* (Amin *et al.*, 2007; Amin and Tucker, 2006; Anthwal and Thompson, 2016). To determine if disruptions in joint specification precede formation of the ectopic cartilage within the incudomalleal joint of *Wnt1-Cre; Fgfr2*$^{flx/flx}$ mice, we examined the incudomalleal joint soon after its establishment at E16.5. Whole mount Alcian blue staining of the malleus and incus showed their separation by an unstained gap in both control and *Wnt1-Cre; Fgfr2*$^{flx/flx}$ embryos, suggesting normal downregulation of chondrogenesis in the developing joint (Figure 7 A, C, arrow) (n=3). Section *in situ* hybridization for the joint specification gene *Gdf5* identified transcripts within the control incudomalleal joint at E16.5. However, in the *Wnt1-Cre; Fgfr2*$^{flx/flx}$ incudomalleal joint, *Gdf5* expression was reduced (Figure 7 B, D, asterisk). Together these results suggest that loss of *Fgfr2* disrupts specification of the incudomalleal joint.

Ectopic bone in the incudomalleal joint of the *Fgfr2* cKO is derived from Scx$^+$ cells

In synovial joints, Gdf5$^+$ cells give rise to the articular cartilage and joint connective tissues, including the joint capsule and intra-articular ligaments (Shwartz *et al.*, 2016). To identify abnormalities in the articular cartilage of the incudomalleal joint, we stained histological sections with Safranin O. In control embryos E18.5, the V-shaped articulation of the malleus and incus was well-delineated and connected by the developing joint capsule (Figure 8A). In *Wnt1-Cre; Fgfr2*$^{flx/flx}$ embryos, the wedge of the incus was largely missing and instead an ectopic chondrogenic element lay within the joint space (Figure 8 C) (n=4). We next employed the *Scx-GFP* reporter to identify abnormalities in the incudomalleal joint connective tissue (Pryce *et al.*, 2007) (Wang *et al.*, 2011). In control embryos at E18.5, *Scx-GFP* marked the intra-articular ligament and joint capsule (Figure 8 B). While *Scx-GFP* marked intra-articular ligament and joint capsule in *Wnt1-Cre; Fgfr2*$^{flx/flx}$ embryos, it was also expressed at low levels in the ectopic cartilage element (Figure 8 D, asterisk) (n=4). These results indicate that ectopic cartilage in the incudomalleal joint space of the *Fgfr2* cKO develops from the Scx$^+$ cells that normally form the joint connective tissues.

To determine if loss of *Fgfr2* plays either an autonomous or non-autonomous role in development of the ectopic cartilage within the *Wnt1-Cre; Fgfr2*$^{flx/flx}$ incudomalleal joint, we examined immunofluorescent localization of Fgfr2 using an antibody that also recognizes the truncated, non-functional protein (Fgfr2Δexons8–10) produced by the recombined *Fgfr2*^{flx} allele. In control embryos at E18.5, Fgfr2$^+$ cells populated the intra-

articular ligaments, joint capsule, and cartilaginous elements of the malleus and incus (Figure 8 B', B") (n=4). In *Wnt1-Cre; Fgfr2*$^{flx/flx}$ embryos, Fgfr2Δexons8–10-expressing cells marked the developing malleus and incus, as well as the ectopic cartilage element within the joint space (Figure 8 D', D", asterisk). Interestingly, cells expressing Fgfr2Δexons8–10 were not detected in the joint capsule and intra-articular ligament of the mutant (Figure 8 D', D", arrow). Together these data suggest that Fgfr2 autonomously regulates differentiation of Scx$^+$ cells during development of the incudomalleal joint.

DISCUSSION

In this study, we demonstrate that *Fgfr2* regulates structure and function of the mammalian middle ear. We show that neural crest-specific knockout of *Fgfr2* induces abnormal development of the skeletal tissues that determine the middle ear's structure, including membranous and endochondral bone and dense connective tissues. Since these skeletal tissues are responsible for the mechanical transmission of sound to the inner ear, disruptions in their development are the likely cause of auditory disfunction in *Fgfr2* cKO mice.

Any one of the multiple defects we identified in the membranous auditory bulla could be responsible for hearing loss in *Fgfr2* cKO mice. The auditory bullae of *Fgfr2* cKO mice were significantly reduced in size and dysmorphic due to hypoplasia of the tympanic ring and retro-tympanic process. The development of the tympanic membrane, an epithelial structure that collects sound at the opening of the middle ear, is highly dependent on proper formation of the tympanic ring (Mallo and Gridley, 1996). Therefore, hypoplasia of the tympanic ring could contribute to conductive hearing loss either directly through its structural role in the auditory bulla or indirectly by affecting development of the tympanic membrane. We also showed that a reduction in the size of the auditory bulla in *Fgfr2* cKO mice corresponds with a reduction in the middle ear air space, delayed cavitation, and direct contact between the manubrium of the malleus and the cochlear wall. Each of these abnormalities is expected to restrict ossicular movement. Confinement of the ossicular chain impedes their ability to vibrate in response to sound and results in conductive hearing loss (Jaisinghani *et al.*, 1999) (Richter *et al.*, 2010).

The defects we identified in the endochondral ossicles and their dense connective tissues could also contribute to hearing loss in *Fgfr2* cKO mice. We found that *Fgfr2* cKO leads to ectopic bone formation on the malleus, incus, and stapes at sites of joint articulation and tendon/ligament attachment. The mobility and suspension of the ossicles depends on the synovial joints that link them, as well as the tendons and ligaments that connect the ossicles to muscles and to the auditory bulla, respectively (Gerig *et al.*, 2015; Wang *et al.*, 2011). Ectopic bone formation in the synovial joints and/or bony fixation of the ossicles to the wall of the auditory bulla limit ossicular movement, block sound transmission, and cause conductive hearing loss (Bartel-Friedrich and Wulke, 2007). We showed that ectopic bone within the incudomalleal joint of *Fgfr2* cKO mice is linked to reduced *Gdf5* expression in the interzone and develops from aberrant differentiation of Scx$^+$ cells into chondrocytes that later undergo endochondral-like ossification. This data indicates that *Fgfr2* regulates differentiation of Scx$^+$ joint progenitor cells, by promoting their expression of *Gdf5* during joint specification. Since Gdf5$^+$/Scx$^+$ progenitor cells also give rise to the connective tissue

of the tendon-to-bone attachment (Dyment *et al.*, 2015), ectopic bone on the *Fgfr2* cKO ossicles at tendon attachment sites can also be explained by this mechanism.

FGF signaling is necessary for many aspects of auditory development (Wright and Mansour, 2003b). Many studies have detailed extraordinarily diverse roles for FGF signaling in the ectoderm and mesoderm during inner ear development (Alvarez *et al.*, 2003; Hatch *et al.*, 2007; Ladher *et al.*, 2005; Urness *et al.*, 2015; Wright and Mansour, 2003a). However, less is known about FGF signaling in middle ear development. Hypoplasia and delayed mineralization of the ossicles have been described in mouse mutants for *Fgfr1* and *Fgfr3* (Brewer *et al.*, 2015; Calvert *et al.*, 2011; Hoch and Soriano, 2006; Pannier *et al.*, 2009). These ossicular phenotypes are quite distinct from those we observe here in the *Fgfr2* cKO mice. Furthermore, defects in the auditory bulla in *Fgfr1* and *Fgfr3* mutant mice have not yet been reported. Together these findings indicate that the developmental role for *Fgfr2* in the middle ear skeleton is unique from that of the other Fgfrs.

The middle ear defects in human congenital disorders resulting from mutations in *FGFR2* underscore the role of the receptor in middle ear development and auditory function. Ossicular hypoplasia and fixation, as well as morphological abnormalities in the auditory bulla, cause conductive hearing loss in the *FGFR2* gain-of-function disorders Apert, Crouzon, and Pfeiffer syndromes (Peterson-Falzone, 1981; Zhou *et al.*, 2009) (Orvidas *et al.*, 1999) (Vallino-Napoli, 1996) (Desai *et al.*, 2010). Conductive and mixed-type hearing loss have been reported in 50% of patients diagnosed with LADD syndrome, a genetically heterogenous disorder that result from loss of function mutations in *FGFR2*, *FGFR3*, and *FGF10* (Rohmann *et al.*, 2006; Shams *et al.*, 2007) (Hollister *et al.*, 1973; Thompson *et al.*, 2012). Clinical reports on LADD syndrome suggest there is a correlation between the genetic heterogeneity and hearing loss. Of the reported LADD syndrome cases with *FGF10* mutations, all patients have normal hearing (Milunsky *et al.*, 2006) (Rohmann *et al.*, 2006). This is consistent with the *FGF10* loss of function disorder Aplasia of lacrimal and salivary glands (ALSG), which presents with normal hearing despite being closely related to LADD syndrome (Entesarian *et al.*, 2007) (Entesarian *et al.*, 2005). Mouse genetics studies also indicate Fgf10 is not required for middle ear development. Fgf10-mediated activation of the epithelial-specific isoform Fgfr2-IIIb, while critical for inner ear development, does not appear to have an effect on the middle ear (Alvarez *et al.*, 2003; De Moerlooze *et al.*, 2000; Ohuchi *et al.*, 2000; Pirvola *et al.*, 2000; Urness *et al.*, 2015). All reported cases of LADD syndrome caused by *FGFR2* and *FGFR3* mutations, on the other hand, have some degree of hearing loss with *FGFR3* mutations being specifically associated with sensorineural hearing loss (Rohmann *et al.*, 2006) (Talebi *et al.*, 2017). Our study suggests that *FGFR2* mutations are largely responsible for cases of LADD syndrome with conductive hearing loss and indicates potential disease etiology.

METHODS

Mice

The $Fgfr2^{flx}$ and *Wnt1-Cre2* driver alleles were previously published and obtained through JAX ($Fgfr2^{flx}$ JAX Stock No. 007569 and *Wnt1-Cre2* JAX Stock No. 022137) (Lewis *et al.*, 2013; Yu *et al.*, 2003). The *Scx-GFP* reporter allele was previously published and made

available by R. Schweitzer (Pryce *et al.*, 2007). Embryonic samples were collected from timed mattings, while postnatal samples were staged according to the date of birth.

Micro-computed tomography (μCT)

μCT scans were performed by the USC Molecular Imaging Center using a μCT50 (Scanco Medical). Samples were rotated at 360° and x-ray settings were standardized to 90 kV and 155 μA. Exposure time of 0.5 seconds per frame generated a nominal resolution of 20 μM. Beam-hardening artifacts were filtered with a 0.5-mm-thick aluminum filter. Amira 6.2 or Avizo 7.1 software packages were used for morphometric analysis. Isosurface renderings of equal threshold were measured using the 3D measuring tool.

Whole mount skeletal preparations

Samples were skinned, eviscerated, and fixed in three changes of 95% ethanol for 3 days. Samples were then incubated in Alcian Blue solution (0.15 mg/ml Alcian Blue 8GX in 80% ethanol and 20% glacial acetic acid) overnight and washed in 95% ethanol for 2 days. Specimens were cleared in a 0.5–1% KOH [w/v] solution for 1–5 days and stained in Alizarin red solution (0.02 mg/ml Alizarin red S, Sigma-Aldrich in 0.5–1% KOH) overnight. Samples were hydrolyzed in a 0.5–1% KOH [w/v] solution for an additional 1–5 days. Stained specimens with cleared tissue were equilibrated in glycerol for imaging.

Auditory brainstem response (ABR) test

ABR testing was conducted on P30 mice according to a previously published protocol (Crow *et al.*, 2015). Mice were anesthetized by intraperitoneal injection of ketamine and xylazine, and body temperature was maintained using the TCAT2DF temperature controller and the HP-4 M heating plate (Physitemp Instruments Inc., Clifton, NJ). During anesthesia, mice received artificial tear ointment. Stainless-steel electrodes were inserted subcutaneously at the vertex of the head and the left mastoid, while a ground electrode was placed at the base of the tail. Test sounds were presented using an Intelligent Hearing Systems speaker attached to an 8-inch-long tube that was inserted into the ear canal. Both left and right ears were assessed. Auditory signals were presented as tones at 4, 8, 16, 24, and 32kHz with a 0.3-ms rise and fall time and a total interval of 1 msec., presented at a rate of 40 signals per second. Signals were sent to an amplifier and then a sound transducer from Intelligent Hearing Systems. Physiologic responses were recorded with a 20,000 analog-to-digital rate and sent to an eight-channel 150-gain AC/DC headbox, and then onto a secondary SynAmps signal amplifier of 2500 gain before analysis. Low pass filter settings were set at 3000 Hz while the high pass filter was set to 100 Hz. Artifact rejection of signals was set at amplitudes exceeding 650 mV. Waveforms (3,000) were averaged at each stimulus intensity. Tone bursts were first presented at a high intensity to elicit a waveform and then the intensity was decreased by 20 dB until nearing the threshold. Intensity was further decreased in smaller steps of 10, 5, and 2 dB as the threshold was approached. The hearing threshold was determined by visual inspection of ABR waveforms and was defined as the intensity at which two peaks could be distinguished. Experiments were replicated at low intensities when the peaks were not apparent.

Auditory canal and bulla measurements

The size of the auditory canal and bulla were measured using the analysis tools provided by the Amira 6.2 or Avizo 7.1 software packages. In brief, auditory canal area were taken from control and *Wnt1-Cre; Fgfr2* $^{flx/flx}$ mutant mice (n=6 for each genotype) in arbitrary units (Au) by quantifying the pixels in the 3D rendered μCT images. Values were normalized to the length of the skull, averaged, and plotted on a log base 10 scale to account for differences in orders of magnitude. To measure the volume of the auditory bulla, the bulla and ossicles were segmented out of the volume and the airspace of the bulla was manually selected from each 20 um ortho-slice that contained the middle ear. The volume of each slice was added together, and Amira was used to calculate the volume in mm^3 of the defined space (n=6). Raw values were averaged and plotted.

Statistical Analyses

All sample measurements were statistically examined by employing a one-way analysis of variance (ANOVA). Mean values plus or minus standard error are plotted. *$p < 0.05$, **$p < 0.01$, ***$p < 0.001$ and ****$p < 0.0001$.

Histology

Tissues were fixed in 4% paraformaldehyde at 4ºC and decalcified with BBC Biochemical Rapid Cal Immuno (Fisher Scientific) overnight at room temperature. Samples were dehydrated in increasing concentrations of ethanol (50%-100%), cleared in Citrisolv (Thermo Scientific), embedded in paraffin, and sectioned in the sagittal plane at 10 μM. Sections were differentially stained with Hall-Brunt quadruple stain (HBQ) (Hall, 1986), Safranin O stain, or Hematoxylin-Eosin stain.

In Situ Hybridization

Gdf5 transcripts were detected within tissue sections using *in situ* hybridization RNAscope Technology (ACD) according to the manufacturer's instructions. Briefly, paraffin sections were baked at 50°C for 1 hour, deparaffinized, washed with 100% EtOH, air dried, and treated with RNAscope hydrogen peroxide for 10 min at RT. Sections were then rinsed with water, treated with antigen retrieval solution for 5 minutes in an Oster Steamer, washed again with water, dehydrated in 100% EtOH, and air dried. Sections were treated with RNAscope Protease Plus digestion at 40°C for 10 min, rinsed in water, and incubated with the mouse *Gdf5* RNAscope probe (#407211) for 2hrs at 40°C. After rinsing with RNAscope wash buffer and incubation with AMP1, AMP2, and AMP3 solutions, the sections were treated with RNAscope Multiplex FL v2 HRP-C1 solution for 15 min at 40°C, washed, and incubated with TSA Cy3 fluorophore at a 1:750 dilution for 30 min at 40°C. Slides were then treated with RNAscope multiplex FL v2 HRP blocker solution for 15 min at RT, washed, mounted with DAPI, and imaged by confocal microscopy.

Immunofluorescence

Specimens at embryonic and postnatal stages were fixed in 4% paraformaldehyde for between 15 minutes and 3 hours, depending on the thickness of the tissue. Postnatal tissues were decalcified with 10% EDTA at pH 7.4 for 1–3 days at 4º C. Embryonic and postnatal

samples were equilibrated overnight with two changes of 30% sucrose/PBS at 4ºC. These samples were then embedded in O.C.T. compound (EMS) and sectioned at 10 μM in the sagittal plane. Frozen sections were washed with PBST (0.1% Tween 20) and blocked with 10% serum for 1 hour at room temperature, then incubated with the rabbit primary anti-BEK antibody (C-17) (sc-122, Santa Cruz, 1:200) and goat primary anti-GFP antibody (ab5450, Abcam, 1:500) overnight at 4ºC. The following day, sections were washed with PBST and incubated with Alexa Fluor secondary antibody at a 1:500 dilution in 10% serum for 1 hour at room temperature. Sections were then washed with PBST and mounted with Vectashield containing DAPI (VWR). Images were taken on the Leica TCS SP5/8 confocal microscope system.

ACKNOWLEDGMENTS

This work was supported by the National Institute of Health [#1R01DE025222 to A.E.M; Diversity Supplement #R01 DE025222-01S1 and #T90DE021982 to R.R.R.; Diversity Supplement #R01 DE025222-02S1 to D.R.]. We thank Rick Friedman and his lab for their technical assistance with ABR testing, Ronen Schweitzer for providing the *Scx-GFP* mouse line, and USC's Molecular Imaging Center for their help with small animal CT imaging. We also thank Francesca Mariani, Creighton Tuzon, and Joanna Salva for their helpful discussions.

Funding: NIDCR #1R01DE025222 to A.E.M

REFERENCES

Aimi K 1983 Role of the tympanic ring in the pathogenesis of congenital cholesteatoma. Laryngoscope 93: 1140–1146. [PubMed: 6888124]

Alvarez Y, Alonso MT, Vendrell V, Zelarayan LC, Chamero P, Theil T, Bosl MR, Kato S, Maconochie M, Riethmacher D, Schimmang T. 2003 Requirements for FGF3 and FGF10 during inner ear formation. Development 130: 6329–6338. [PubMed: 14623822]

Amin S, Matalova E, Simpson C, Yoshida H, Tucker AS. 2007 Incudomalleal joint formation: the roles of apoptosis, migration and downregulation. BMC Dev Biol 7: 134. [PubMed: 18053235]

Amin S, Tucker AS. 2006 Joint formation in the middle ear: lessons from the mouse and guinea pig. Dev Dyn 235: 1326–1333. [PubMed: 16425222]

Anthwal N, Thompson H. 2016 The development of the mammalian outer and middle ear. J Anat 228: 217–232. [PubMed: 26227955]

Bartel-Friedrich S, Wulke C. 2007 Classification and diagnosis of ear malformations. GMS Curr Top Otorhinolaryngol Head Neck Surg 6: Doc05.

Brewer JR, Molotkov A, Mazot P, Hoch RV, Soriano P. 2015 Fgfr1 regulates development through the combinatorial use of signaling proteins. Genes Dev 29: 1863–1874. [PubMed: 26341559]

Calvert JA, Dedos SG, Hawker K, Fleming M, Lewis MA, Steel KP. 2011 A missense mutation in Fgfr1 causes ear and skull defects in hush puppy mice. Mamm Genome 22: 290–305. [PubMed: 21479780]

Cordas EA, Ng L, Hernandez A, Kaneshige M, Cheng SY, Forrest D. 2012 Thyroid hormone receptors control developmental maturation of the middle ear and the size of the ossicular bones. Endocrinology 153: 1548–1560. [PubMed: 22253431]

Crow AL, Ohmen J, Wang J, Lavinsky J, Hartiala J, Li Q, Li X, Salehide P, Eskin E, Pan C, Lusis AJ, Allayee H, Friedman RA. 2015 The Genetic Architecture of Hearing Impairment in Mice: Evidence for Frequency-Specific Genetic Determinants. G3 (Bethesda) 5: 2329–2339. [PubMed: 26342000]

De Moerlooze L, Spencer-Dene B, Revest JM, Hajihosseini M, Rosewell I, Dickson C. 2000 An important role for the IIIb isoform of fibroblast growth factor receptor 2 (FGFR2) in mesenchymal-epithelial signalling during mouse organogenesis. Development 127: 483–492. [PubMed: 10631169]

Desai U, Rosen H, Mulliken JB, Gopen Q, Meara JG, Rogers GF. 2010 Audiologic findings in Pfeiffer syndrome. J Craniofac Surg 21: 1411–1418. [PubMed: 20856029]

Dyment NA, Breidenbach AP, Schwartz AG, Russell RP, Aschbacher-Smith L, Liu H, Hagiwara Y, Jiang R, Thomopoulos S, Butler DL, Rowe DW. 2015 Gdf5 progenitors give rise to fibrocartilage cells that mineralize via hedgehog signaling to form the zonal enthesis. Dev Biol 405: 96–107. [PubMed: 26141957]

Entesarian M, Dahlqvist J, Shashi V, Stanley CS, Falahat B, Reardon W, Dahl N. 2007 FGF10 missense mutations in aplasia of lacrimal and salivary glands (ALSG). Eur J Hum Genet 15: 379–382. [PubMed: 17213838]

Entesarian M, Matsson H, Klar J, Bergendal B, Olson L, Arakaki R, Hayashi Y, Ohuchi H, Falahat B, Bolstad AI, Jonsson R, Wahren-Herlenius M, Dahl N. 2005 Mutations in the gene encoding fibroblast growth factor 10 are associated with aplasia of lacrimal and salivary glands. Nat Genet 37: 125–127. [PubMed: 15654336]

Gerig R, Ihrle S, Roosli C, Dalbert A, Dobrev I, Pfiffner F, Eiber A, Huber AM, Sim JH. 2015 Contribution of the incudo-malleolar joint to middle-ear sound transmission. Hear Res 327: 218–226. [PubMed: 26209186]

Hall BK. 1986 The role of movement and tissue interactions in the development and growth of bone and secondary cartilage in the clavicle of the embryonic chick. J Embryol Exp Morphol 93: 133–152. [PubMed: 3734681]

Hall BK, Miyake T. 2000 All for one and one for all: condensations and the initiation of skeletal development. Bioessays 22: 138–147. [PubMed: 10655033]

Hatch EP, Noyes CA, Wang X, Wright TJ, Mansour SL. 2007 Fgf3 is required for dorsal patterning and morphogenesis of the inner ear epithelium. Development 134: 3615–3625. [PubMed: 17855431]

Hoch RV, Soriano P. 2006 Context-specific requirements for Fgfr1 signaling through Frs2 and Frs3 during mouse development. Development 133: 663–673. [PubMed: 16421190]

Hollister DW, Klein SH, De Jager HJ, Lachman RS, Rimoin DL. 1973 The lacrimo-auriculo-dento-digital syndrome. J Pediatr 83: 438–444. [PubMed: 4725147]

Jaisinghani VJ, Paparella MM, Schachern PA, Schneider DS, Le CT. 1999 Residual mesenchyme persisting into adulthood. Am J Otolaryngol 20: 363–370. [PubMed: 10609480]

Ladher RK, Wright TJ, Moon AM, Mansour SL, Schoenwolf GC. 2005 FGF8 initiates inner ear induction in chick and mouse. Genes Dev 19: 603–613. [PubMed: 15741321]

Lewis AE, Vasudevan HN, O'Neill AK, Soriano P, Bush JO. 2013 The widely used Wnt1-Cre transgene causes developmental phenotypes by ectopic activation of Wnt signaling. Dev Biol 379: 229–234. [PubMed: 23648512]

Mallo M, Gridley T. 1996 Development of the mammalian ear: coordinate regulation of formation of the tympanic ring and the external acoustic meatus. Development 122: 173–179. [PubMed: 8565828]

Milunsky JM, Zhao G, Maher TA, Colby R, Everman DB. 2006 LADD syndrome is caused by FGF10 mutations. Clin Genet 69: 349–354. [PubMed: 16630169]

Minoux M, Kratochwil CF, Ducret S, Amin S, Kitazawa T, Kurihara H, Bobola N, Vilain N, Rijli FM. 2013 Mouse Hoxa2 mutations provide a model for microtia and auricle duplication. Development 140: 4386–4397. [PubMed: 24067355]

Mori-Akiyama Y, Akiyama H, Rowitch DH, de Crombrugghe B. 2003 Sox9 is required for determination of the chondrogenic cell lineage in the cranial neural crest. Proc Natl Acad Sci U S A 100: 9360–9365. [PubMed: 12878728]

Noben-Trauth K, Johnson KR. 2009 Inheritance patterns of progressive hearing loss in laboratory strains of mice. Brain Res 1277: 42–51. [PubMed: 19236853]

O'Gorman S 2005 Second branchial arch lineages of the middle ear of wild-type and Hoxa2 mutant mice. Dev Dyn 234: 124–131. [PubMed: 15861402]

Ohuchi H, Hori Y, Yamasaki M, Harada H, Sekine K, Kato S, Itoh N. 2000 FGF10 acts as a major ligand for FGF receptor 2 IIIb in mouse multi-organ development. Biochem Biophys Res Commun 277: 643–649. [PubMed: 11062007]

Orvidas LJ, Fabry LB, Diacova S, McDonald TJ. 1999 Hearing and otopathology in Crouzon syndrome. Laryngoscope 109: 1372–1375. [PubMed: 10499038]

Pannier S, Couloigner V, Messaddeq N, Elmaleh-Berges M, Munnich A, Romand R, Legeai-Mallet L. 2009 Activating Fgfr3 Y367C mutation causes hearing loss and inner ear defect in a mouse model of chondrodysplasia. Biochim Biophys Acta 1792: 140–147. [PubMed: 19073250]

Peterson-Falzone SJ. 1981 Impact of communicative disorders on otolaryngologic care of patients with craniofacial anomalies. Otolaryngol Clin North Am 14: 895–915. [PubMed: 7335363]

Pirvola U, Spencer-Dene B, Xing-Qun L, Kettunen P, Thesleff I, Fritzsch B, Dickson C, Ylikoski J. 2000 FGF/FGFR-2(IIIb) signaling is essential for inner ear morphogenesis. J Neurosci 20: 6125–6134. [PubMed: 10934262]

Pryce BA, Brent AE, Murchison ND, Tabin CJ, Schweitzer R. 2007 Generation of transgenic tendon reporters, ScxGFP and ScxAP, using regulatory elements of the scleraxis gene. Dev Dyn 236: 1677–1682. [PubMed: 17497702]

Richter CA, Amin S, Linden J, Dixon J, Dixon MJ, Tucker AS. 2010 Defects in middle ear cavitation cause conductive hearing loss in the Tcof1 mutant mouse. Hum Mol Genet 19: 1551–1560. [PubMed: 20106873]

Rijli FM, Mark M, Lakkaraju S, Dierich A, Dolle P, Chambon P. 1993 A homeotic transformation is generated in the rostral branchial region of the head by disruption of Hoxa-2, which acts as a selector gene. Cell 75: 1333–1349. [PubMed: 7903601]

Rohmann E, Brunner HG, Kayserili H, Uyguner O, Nurnberg G, Lew ED, Dobbie A, Eswarakumar VP, Uzumcu A, Ulubil-Emeroglu M, Leroy JG, Li Y, Becker C, Lehnerdt K, Cremers CW, Yuksel-Apak M, Nurnberg P, Kubisch C, Schlessinger J, van Bokhoven H, Wollnik B. 2006 Mutations in different components of FGF signaling in LADD syndrome. Nat Genet 38: 414–417. [PubMed: 16501574]

Settle SH, Jr., Rountree RB, Sinha A, Thacker A, Higgins K, Kingsley DM. 2003 Multiple joint and skeletal patterning defects caused by single and double mutations in the mouse Gdf6 and Gdf5 genes. Dev Biol 254: 116–130. [PubMed: 12606286]

Shams I, Rohmann E, Eswarakumar VP, Lew ED, Yuzawa S, Wollnik B, Schlessinger J, Lax I. 2007 Lacrimo-auriculo-dento-digital syndrome is caused by reduced activity of the fibroblast growth factor 10 (FGF10)-FGF receptor 2 signaling pathway. Mol Cell Biol 27: 6903–6912. [PubMed: 17682060]

Shwartz Y, Viukov S, Krief S, Zelzer E. 2016 Joint Development Involves a Continuous Influx of Gdf5-Positive Cells. Cell Rep 15: 2577–2587. [PubMed: 27292641]

Talebi F, Ghanbari Mardasi F, Mohammadi Asl J, Bavarsad AH, Tizno S. 2017 Identification of a novel missence mutation in FGFR3 gene in an Iranian family with LADD syndrome by Next-Generation Sequencing. Int J Pediatr Otorhinolaryngol 97: 192–196. [PubMed: 28483234]

Thompson E, Pembrey M, Graham JM. 1985 Phenotypic variation in LADD syndrome. J Med Genet 22: 382–385. [PubMed: 4078868]

Thompson H, Ohazama A, Sharpe PT, Tucker AS. 2012 The origin of the stapes and relationship to the otic capsule and oval window. Dev Dyn 241: 1396–1404. [PubMed: 22778034]

Trokovic N, Trokovic R, Mai P, Partanen J. 2003 Fgfr1 regulates patterning of the pharyngeal region. Genes Dev 17: 141–153. [PubMed: 12514106]

Urness LD, Wang X, Shibata S, Ohyama T, Mansour SL. 2015 Fgf10 is required for specification of non-sensory regions of the cochlear epithelium. Dev Biol 400: 59–71. [PubMed: 25624266]

Vallino-Napoli LD. 1996 Audiologic and otologic characteristics of Pfeiffer syndrome. Cleft Palate Craniofac J 33: 524–529. [PubMed: 8939381]

Wang L, Bresee CS, Jiang H, He W, Ren T, Schweitzer R, Brigande JV. 2011 Scleraxis is required for differentiation of the stapedius and tensor tympani tendons of the middle ear. J Assoc Res Otolaryngol 12: 407–421. [PubMed: 21399989]

Willott JF, Turner JG. 1999 Prolonged exposure to an augmented acoustic environment ameliorates age-related auditory changes in C57BL/6J and DBA/2J mice. Hear Res 135: 78–88. [PubMed: 10491957]

Wright TJ, Mansour SL. 2003a Fgf3 and Fgf10 are required for mouse otic placode induction. Development 130: 3379–3390. [PubMed: 12810586]

Wright TJ, Mansour SL. 2003b FGF signaling in ear development and innervation. Curr Top Dev Biol 57: 225–259. [PubMed: 14674483]

Xu PX, Adams J, Peters H, Brown MC, Heaney S, Maas R. 1999 Eya1-deficient mice lack ears and kidneys and show abnormal apoptosis of organ primordia. Nat Genet 23: 113–117. [PubMed: 10471511]

Yu K, Xu J, Liu Z, Sosic D, Shao J, Olson EN, Towler DA, Ornitz DM. 2003 Conditional inactivation of FGF receptor 2 reveals an essential role for FGF signaling in the regulation of osteoblast function and bone growth. Development 130: 3063–3074. [PubMed: 12756187]

Zhou G, Schwartz LT, Gopen Q. 2009 Inner ear anomalies and conductive hearing loss in children with Apert syndrome: an overlooked otologic aspect. Otol Neurotol 30: 184–189. [PubMed: 19169132]

Zhou X, Jen PH, Seburn KL, Frankel WN, Zheng QY. 2006 Auditory brainstem responses in 10 inbred strains of mice. Brain Res 1091: 16–26. [PubMed: 16516865]

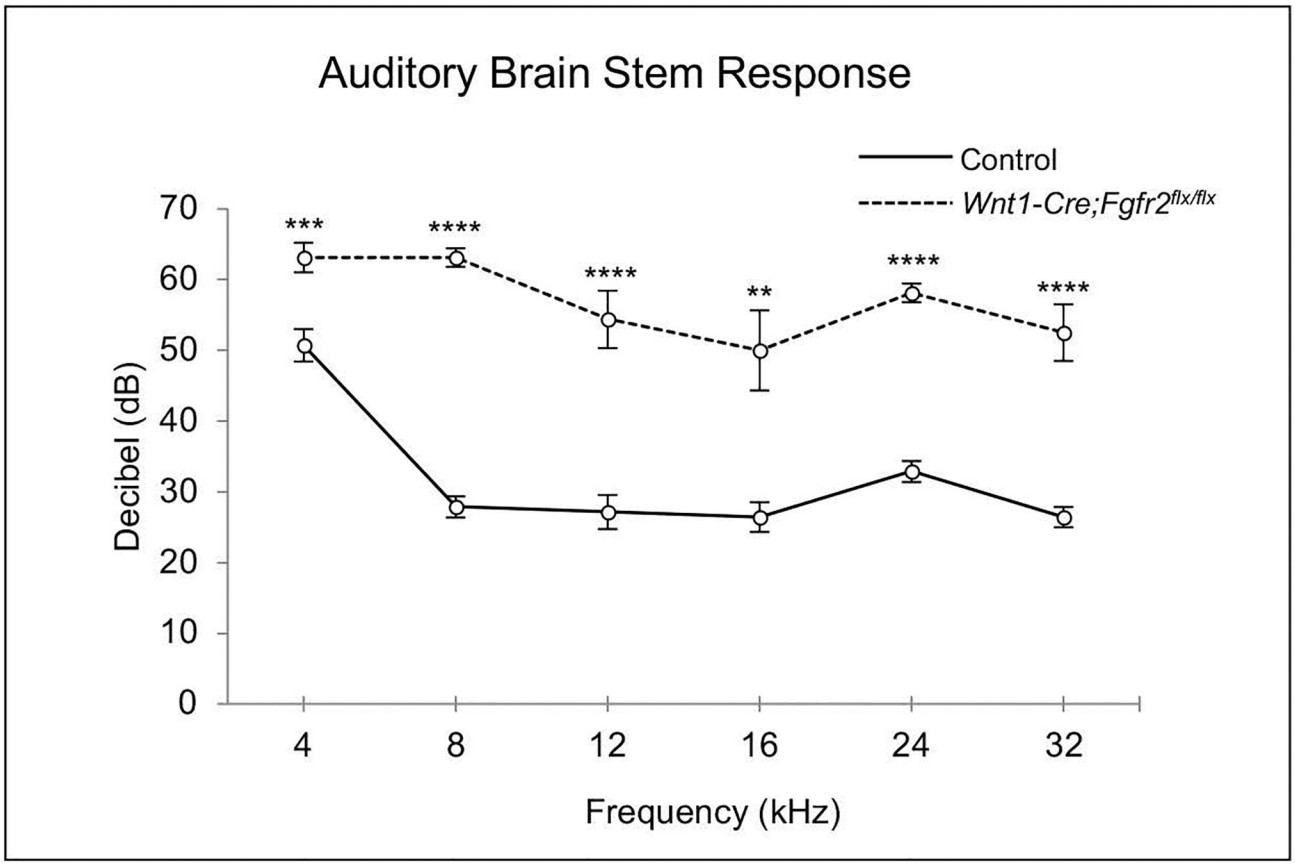

Figure 1.

Wnt1-Cre; Fgfr2$^{flx/flx}$ mice have decreased auditory function. Auditory Brainstem Response (ABR) testing of control and *Wnt1-Cre; Fgfr2*$^{flx/flx}$ littermates at P30 (n=6). Mean values plus or minus standard error are plotted. $^{**}p < 0.01$, $^{***}p < 0.001$ and $^{****}p < 0.0001$.

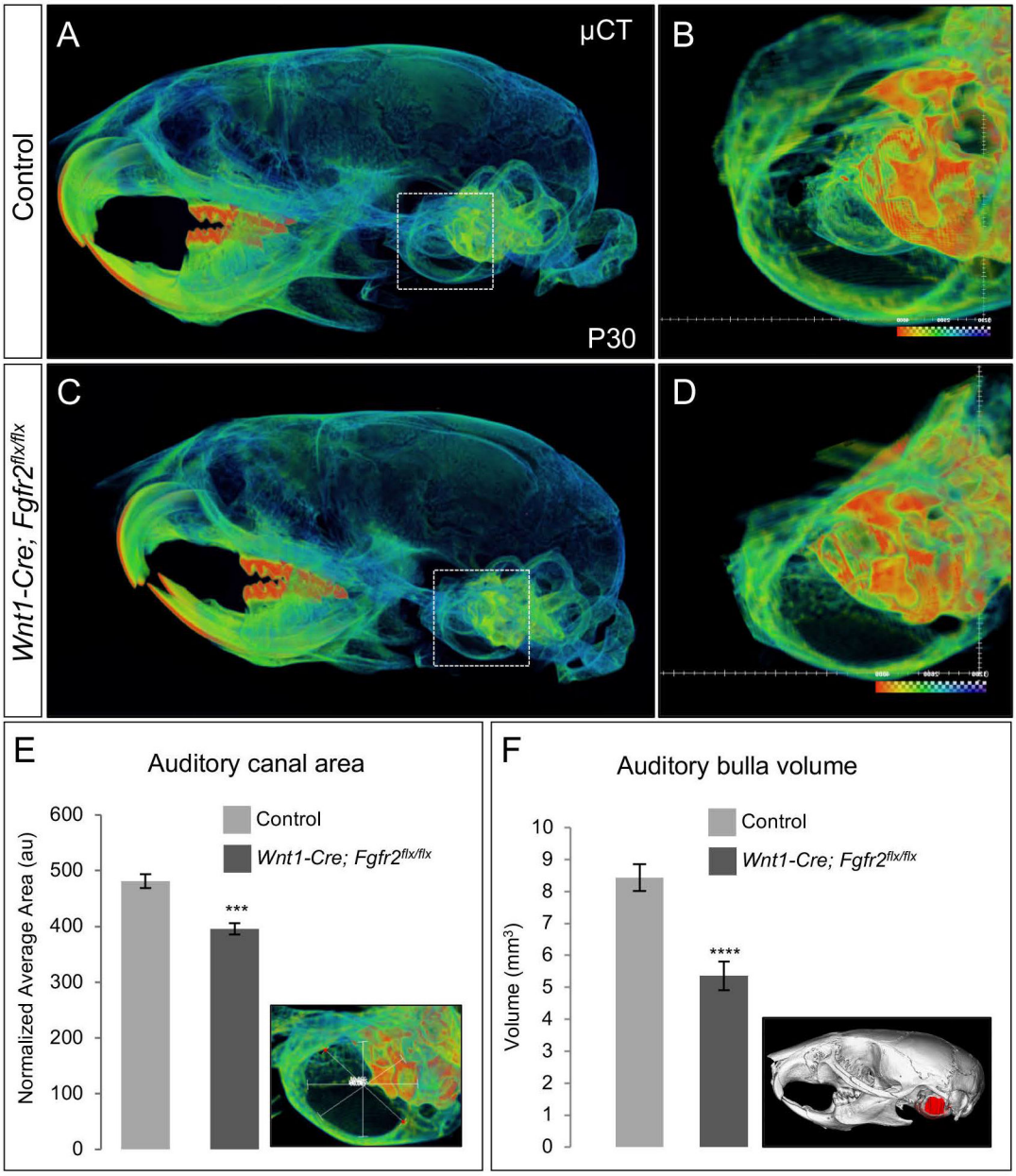

Figure 2.

The auditory bulla is dysmorphic in *Wnt1-Cre; Fgfr2*$^{flx/flx}$ mice. (A, C) μCT of P30 skulls of control and *Wnt1-Cre; Fgfr2*$^{flx/flx}$ littermates (n=3). (B, D) Higher magnification rendering of tympanic bulla and middle ear ossicles (boxed regions from A and C). (E) Measurements of the auditory canal area from control and *Wnt1-Cre; Fgfr2*$^{flx/flx}$ littermates (n=3). Lines in the inset image shows the area measured. (E) Measurements of the auditory bulla volume from control and *Wnt1-Cre; Fgfr2*$^{flx/flx}$ littermates (n=3), as shown in the inset image. ***$p < 0.001$ and ****$p < 0.0001$.

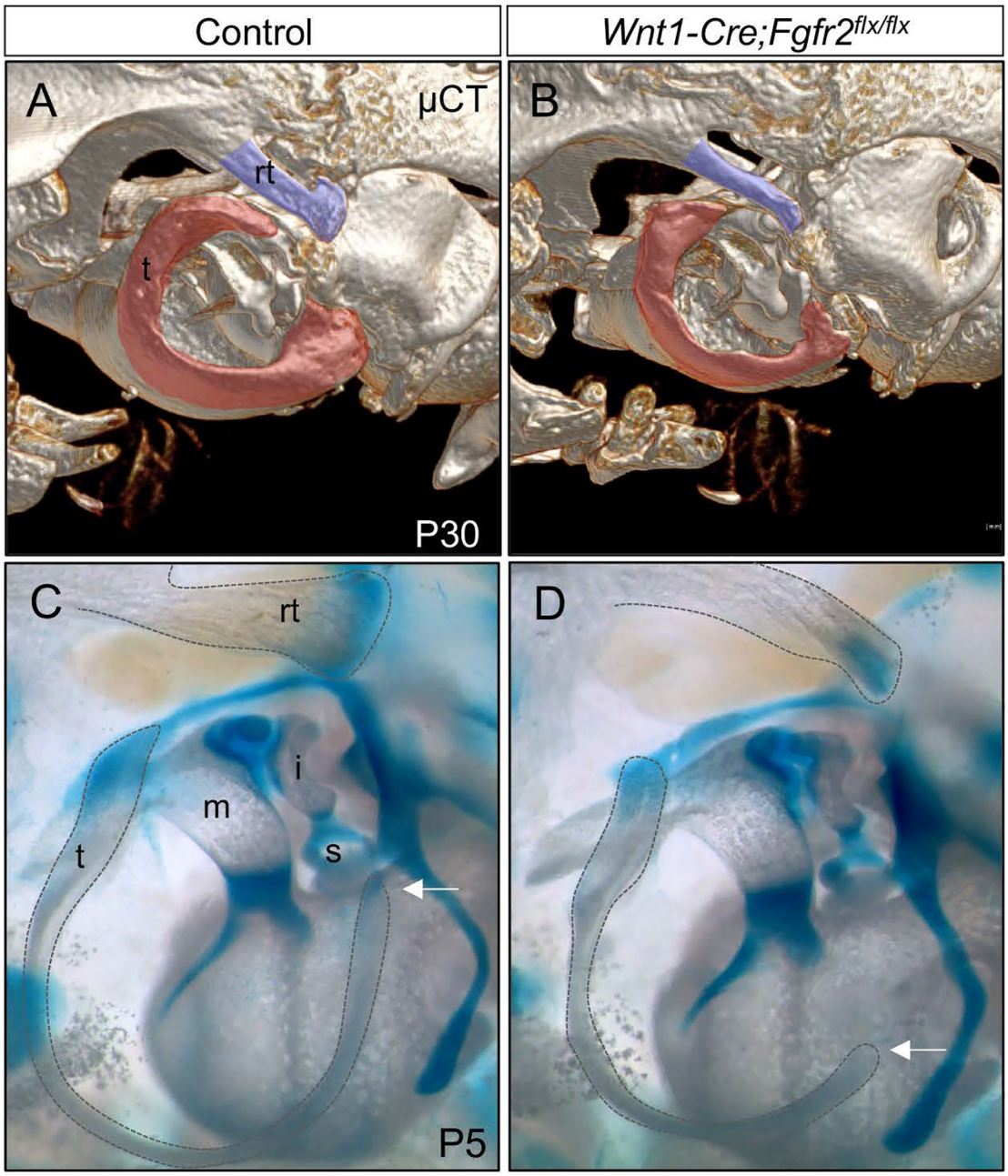

Figure 3.

The tympanic ring and retrotympanic process are hypoplastic in *Wnt1-Cre; Fgfr2*$^{flx/flx}$ mice. (A, B) Sagittal surface μCT rendering of the auditory bulla in control and *Wnt1-Cre; Fgfr2*$^{flx/flx}$ littermates at P30 (n=3). The tympanic ring is pseudo-colored red and retrotympanic process is pseudo-colored blue. (C, D) Alcian blue cartilage stain of the developing auditory bulla in control and *Wnt1-Cre; Fgfr2*$^{flx/flx}$ littermates at P5 (n=3). The membrane bones of the retrotympanic process and tympanic ring are demarcated with dotted lines. The white arrow indicates the most dorsal tip of the tympanic ring. i, incus; m, malleus; rt, retrotympanic process; s, stapes; and t, tympanic ring.

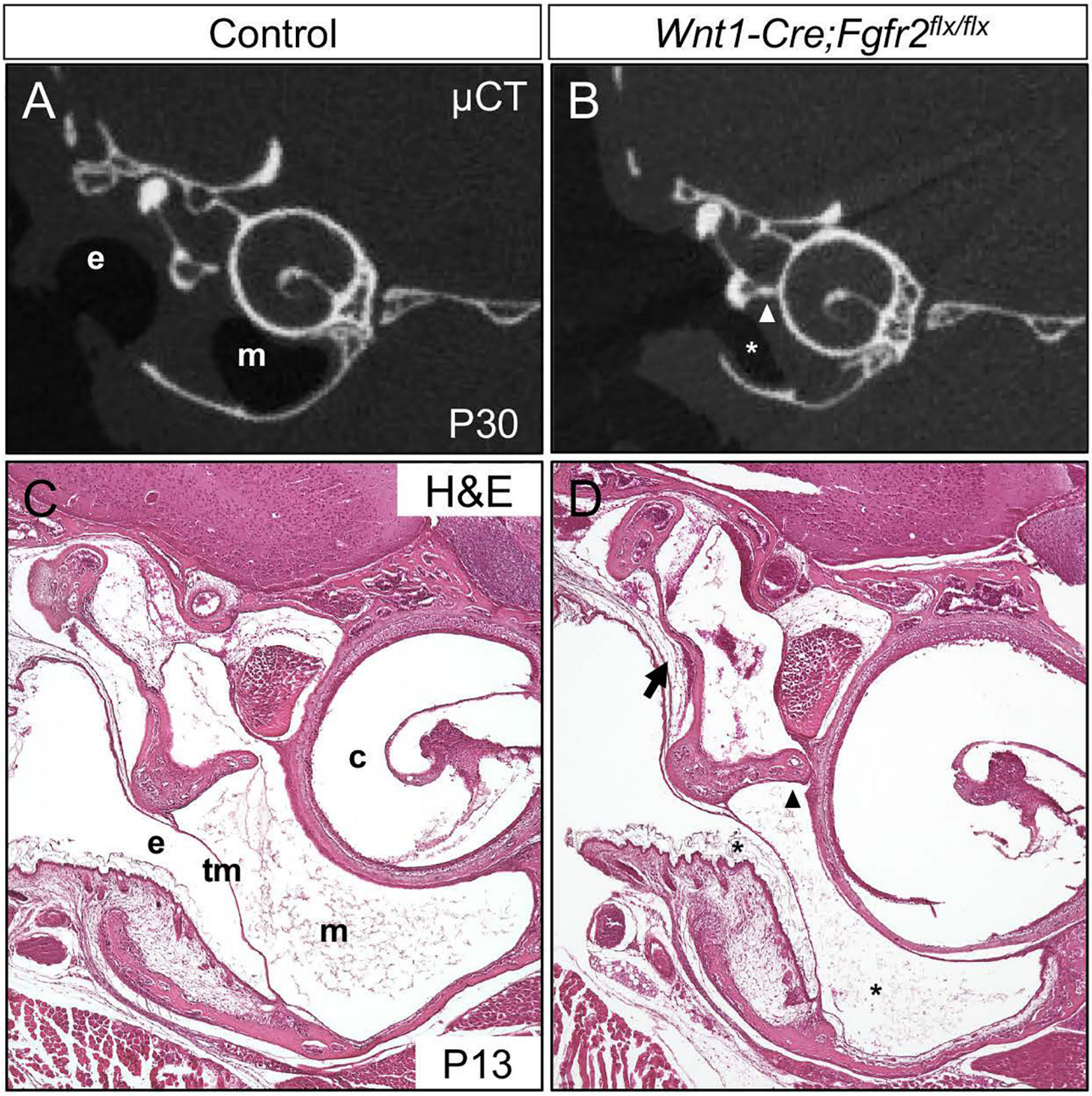

Figure 4.

The airspace cavities in *Wnt1-Cre; Fgfr2*$^{flx/flx}$ mice are reduced in size and dysmorphic. (A, B) Coronal orthogonal μCT slices through the middle ear at P30 in control and *Wnt1-Cre; Fgfr2*$^{flx/flx}$ littermates (n=3). The cavities of the external (e) and middle ear (m) are indicated in the control. Asterisk denotes abnormal middle ear airspace in mutant. (C, D) Histological sections stained with Hematoxylin-Eosin at P13 in control and *Wnt1-Cre; Fgfr2*$^{flx/flx}$ littermates (n=3). In panel D, the asterisks indicate abnormalities in the ear air space, arrowheads show the close proximity of the malleus to the cochlea, and the arrow marks

mesenchymal adhesion between the tympanic membrane and malleus. c, cochlea; e, external ear cavity; m, middle ear cavity; and tm, tympanic membrane.

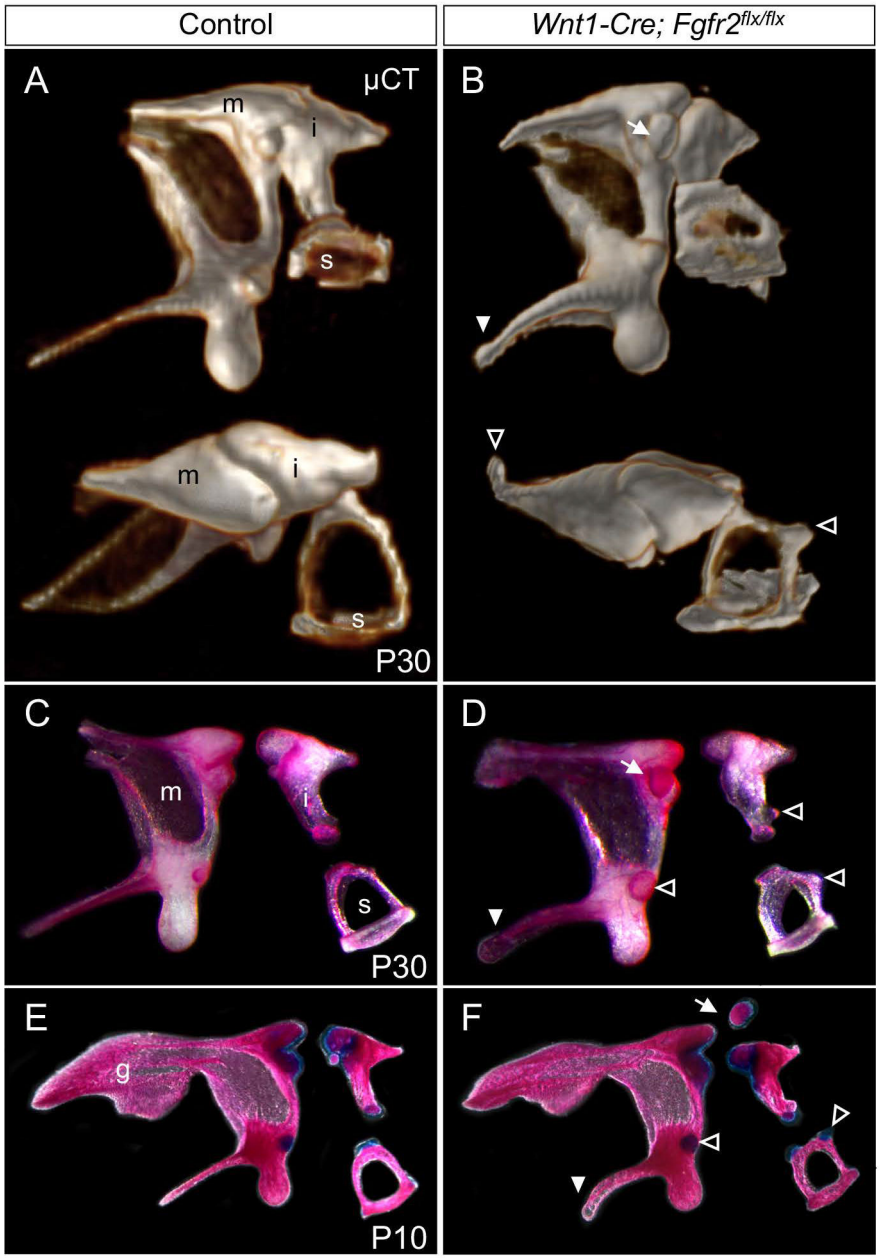

Figure 5.

The ossicles of *Wnt1-Cre; Fgfr2*$^{flx/flx}$ mice exhibit ectopic bone at the sites of tendon/ligament attachment and within the incudomalleal joint. (A, B) μCT renderings of the internal and base surfaces of the ear ossicles at P30 in control and *Wnt1-Cre; Fgfr2*$^{flx/flx}$ littermates (n = 3). Alizarin red and Alcian blue staining of ossicles disarticulated from control and *Wnt1-Cre; Fgfr2*$^{flx/flx}$ littermates at P30 (C, D) (n = 3) and P10 (E, F) (n = 3). Open arrowheads indicate ectopic bone at tendon/ligament attachment sites, arrows mark the ectopic bone nodule within the incudomalleal joint, and arrowheads denote ectopic bone on the manubrium. i, incus; m, malleus; and s, stapes.

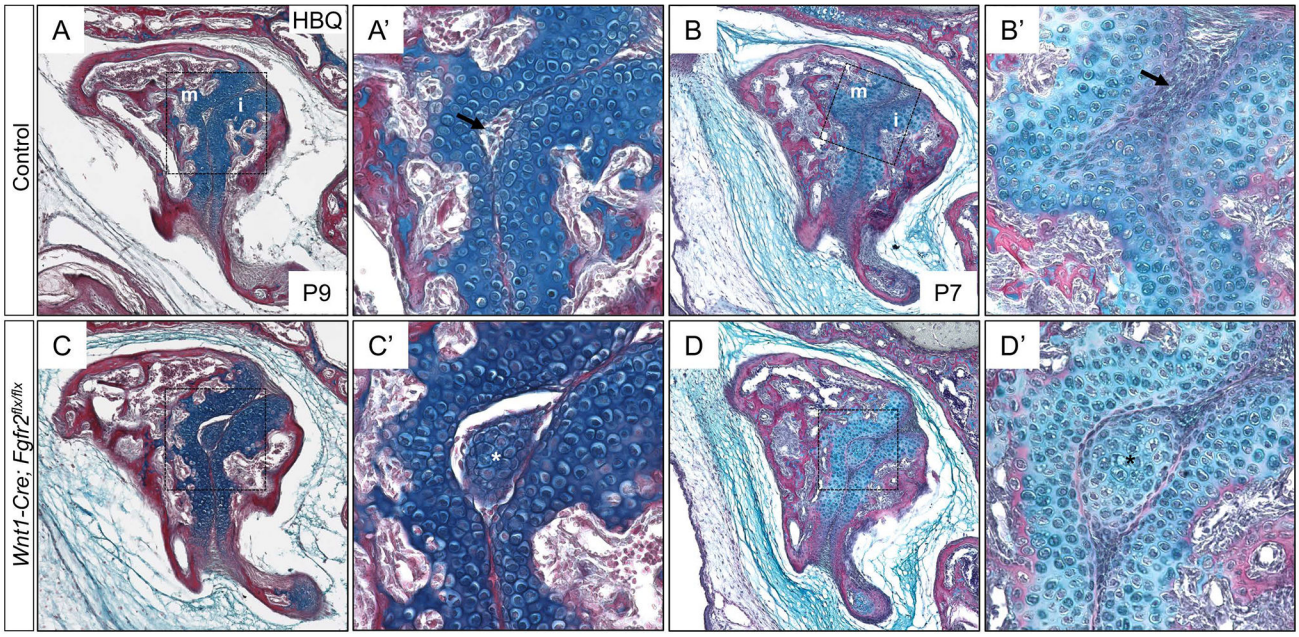

Figure 6.

Ectopic cartilage forms within the synovial joint between the malleus and incus in *Wnt1-Cre; Fgfr2*$^{flx/flx}$ mice. Histological sections of the middle ear stained with HBQ at P9 (A, C) (n=4) and P7 (B, D) (n=4) in control and *Wnt1-Cre; Fgfr2*$^{flx/flx}$ littermates. A'-D' are higher magnification images of the incudomalleal joint region demarcated by the boxes in their corresponding lower magnification images. Arrows indicate normal joint space and asterisks mark the ectopic cartilage nodule. i, incus; and m, malleus.

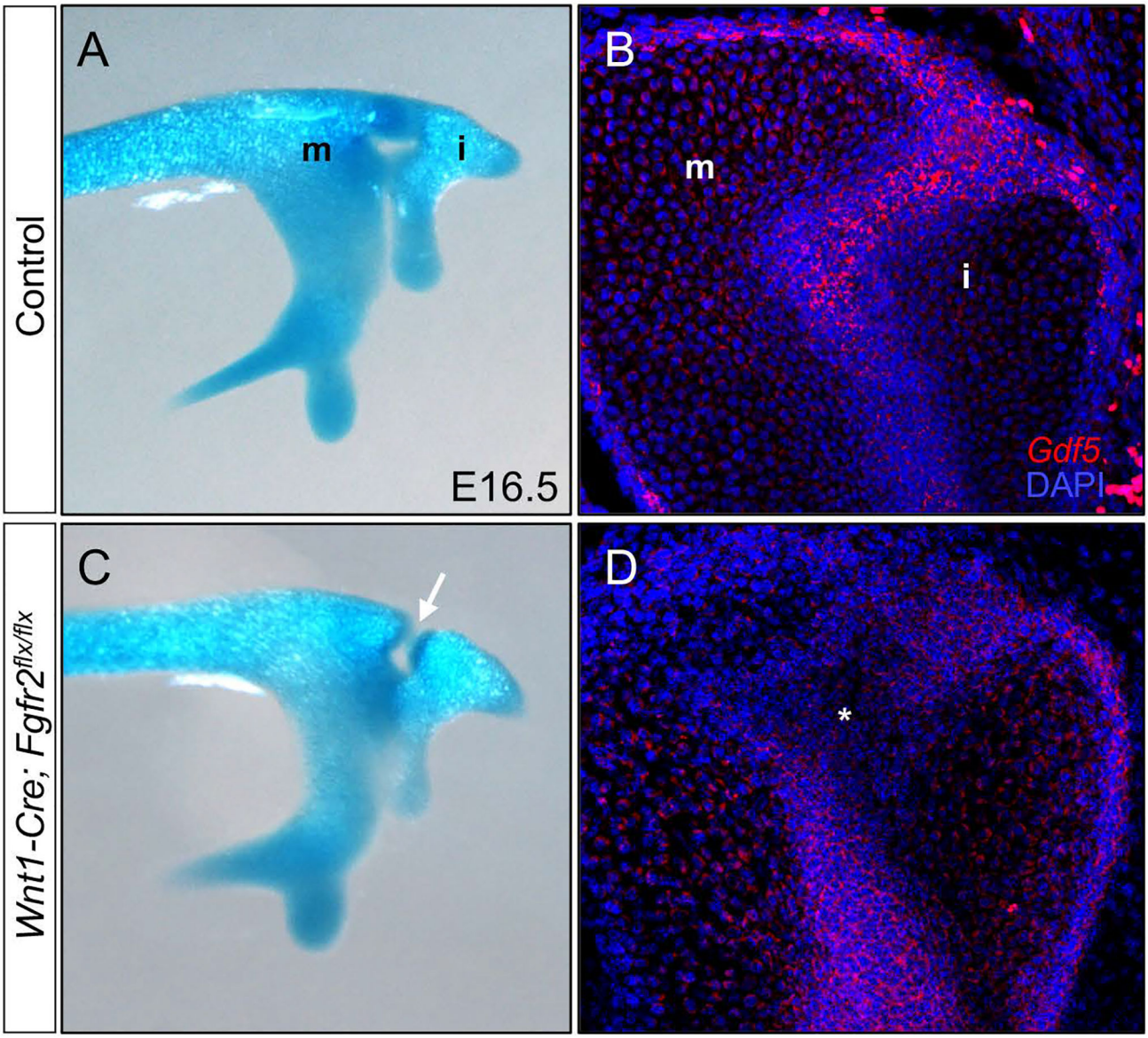

Figure 7.

Specification of incudomalleal joint is abnormal in *Wnt1-Cre; Fgfr2*$^{flx/flx}$ embryos (A, C) Whole mount Alcian blue staining of the cartilage anlagen for the malleus and incus at E16.5 in control and *Wnt1-Cre; Fgfr2*$^{flx/flx}$ embryos (n=3). (B, D) Section *in situ* hybridization of *Gdf5* in the incudomalleal joint at E16.5 in control and *Wnt1-Cre; Fgfr2*$^{flx/flx}$ embryos (n=3). Arrow indicates the developing incudomalleal joint. In panel D, the asterisk indicates reduced *Gdf5* expression in the joint interzone. i, incus; and m, malleus.

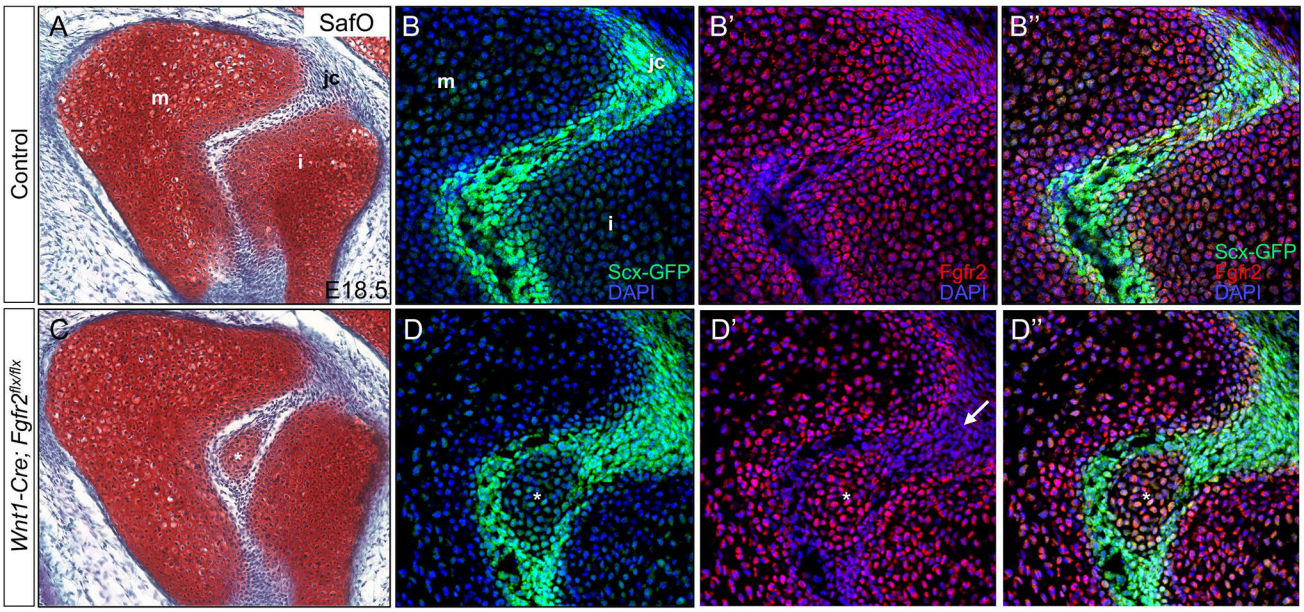

Figure 8.

Ectopic cartilage within incudomalleal joint of *Wnt1-Cre; Fgfr2*$^{flx/flx}$ develops from Scx^{+} cells. (A, C) Safranin O staining of the incudomalleal joint at E18.5 in control and *Wnt1-Cre; Fgfr2*$^{flx/flx}$ embryos (n=4). (B, D) Immunofluorescent staining for *Scx-GFP* (green)(B, B") and anti-Fgfr2 (red)(B', B") in the incudomalleal joint at E18.5 in control and *Wnt1-Cre; Fgfr2*$^{flx/flx}$ embryos (n=4). In panels C, D, D' and D", the asterisks indicate the developing ectopic cartilage. i, incus; jc, joint capsule; and m, malleus.